

Design of Magnetic Coupler for AUV Wireless Charging and Its Electromagnetic Field Simulation

YAN Jiapeng, TANG Wei, WANG Xu, WANG Jia, CHEN Hanwei

Jiangsu University of Science and Technology, Zhenjiang City, Jiangsu Province, China, 212100;

Abstract. The magnetic coupler is one of the important components of wireless charging system, and its coupling coefficient directly influences the energy transmission efficiency. This paper designs a magnetic coupler for Autonomous Underwater Vehicle(AUV) wireless charging in the marine environment. Firstly, the eddy current effect during energy transmission of the magnetic coupler under seawater conditions is analyzed, and the equivalent model of the wireless charging system is compensated and corrected. Then, the genetic-BP neural network algorithm is used to determine the relevant structural parameters of the magnetic coupler. Finally, the electromagnetic field simulation analysis of the offset phenomenon between the transmitting and receiving sides of the magnetic coupler is carried out based on ANSYS MAXEWELL software. The results show that the coupling coefficient of the magnetic coupler under normal operation is 0.87, and if there is a 10mm radial offset (or 5 ° circumferential offset), the coupling coefficient will decrease to 0.74 (or 0.78), which provides a reference basis for the subsequent offset fault-tolerant design of the AUV wireless charging system.

Keywords: underwater wireless charging; magnetic coupler; structural parameters; electromagnetic field simulation

1. Introduction

Wireless Power Transfer (WPT) technology, capable of achieving a well-established electrical isolation between power source and load, has found extensive applications in various fields such as electric vehicles, mobile robots, and consumer electronics. Autonomous Underwater Vehicles (AUVs), as crucial tools for human exploration and utilization of the ocean, face limitations in their ability to conduct prolonged underwater missions and operations due to the constraints imposed by the capacity of energy storage batteries. In conventional operational modes, AUVs are required to periodically surface to replenish energy through connections to surface vessels, platforms, or nearshore cables, resulting in drawbacks such as low operational efficiency and insufficient stealth.

The prospect of underwater wireless charging for AUVs holds great promise, as it can effectively eliminate issues related to cable entanglement between AUVs and charging stations in the marine environment. Furthermore, it addresses safety concerns associated with traditional wet-plug charging methods, such as sparks and leakage, providing a comprehensive solution. Additionally, underwater wireless charging has the potential to significantly enhance the operational continuity and stealthiness of AUVs. Therefore, underwater wireless charging technology demonstrates broad prospects for application in this domain.

Magnetic couplers are a crucial component of underwater wireless charging systems, and conducting research on their design is beneficial not only for enhancing energy transfer efficiency under seawater conditions but also for minimizing the interference caused by charging-induced magnetic fields on AUV control systems [1-4]. In general, the design of magnetic couplers encompasses two aspects: the structural design of the coupler and the determination of structural parameters. The former dictates the mechanical coupling between the wireless charging system's transmitting and receiving sides, while the latter directly affects the magnetic coupling coefficient between the two sides and the overall charging efficiency of the system [5-6].

In recent years, some scholars both domestically and internationally have made meaningful explorations in the design of magnetic couplers. Kan T et al. [7] designed a three-phase rotating wireless charging system, where the involved magnetic coupler consists of three sets of transmitters and receivers. The coupler's configuration utilizes a discrete three-phase resonant coil distinct from

penetrating complete circular coils. However, due to the dispersed relative positions of the receiving and transmitting coils, the receiver coil cannot fully harness the magnetic field energy from the transmitting side. Teeneti C R et al. [8] applied Inductive Wireless Power Transfer (IWPT) technology to AUV wireless charging systems and conducted in-depth analyses of seawater conductivity and the impact of water flow. However, these research findings were not specifically applied to the design of magnetic couplers for a particular AUV. Agostinho L R et al. [9] designed a funnel-shaped magnetic coupler structure, advantageous for installation and less sensitive to misalignment, effectively improving the stability of wireless charging. Nevertheless, the installation of this coupler requires modification to the AUV's head, potentially increasing resistance during AUV navigation. Wang Zhongda [10] designed an AUV wireless charging system from the perspectives of electromagnetic coupling mechanisms, resonant compensation networks, and closed-loop control systems. The coupler evolved from the traditional E-shaped loosely coupled transformer, but its adoption of the E-shaped structure does not adapt well to the AUV's curved exterior, often causing abrupt changes in the magnetic field at the edges and resulting in uneven local magnetic flux leakage. Qin Mu [11] designed a magnetic coupler device with redundant magnetic cores and coils, achieving a tolerance range of $\pm 14^\circ$ in the rotational direction and $\pm 25\text{mm}$ in the axial direction. However, this coupler introduces a certain degree of human error, as it cannot guarantee that the coupling coefficients and inductance values of the two sets of coupler devices are entirely identical, necessitating further research. Cai Chunwei [12] proposed a magnetic coupler based on dipole coil technology, employing a novel circumferential coupling method. The magnetic flux is entirely limited by the coupling method, and through size optimization, lightweight design is achieved. However, a thorough analysis of the impact of seawater medium was not conducted.

The aforementioned studies by predecessors provide some directional guidance for this paper. Combining the main analysis of oceanic conditions, this paper primarily analyzes the equivalent model of wireless charging under the influence of eddy current effects and designs magnetic couplers specifically for AUV wireless charging. From the perspective of adapting to the AUV's exterior structure and the influence of DD coil-coupled magnetic field zoning on the coupling coefficient, the structural form of the entire coupler is designed. The genetic algorithm is used to optimize the BP neural network to determine the relevant structural parameters of the magnetic coupler coils and ferrites in the MATLAB environment. Finite element simulation of the magnetic field distribution of the magnetic coupler is performed using ANSYS MAXWELL software, with a particular focus on analyzing the influence of radial and circumferential offsets during AUV charging on the magnetic coupling coefficient. This analysis provides necessary insights for the subsequent design of offset tolerance in the magnetic coupler.

2. Underwater wireless charging equivalent model in seawater conditions

2.1 Section Headings

2.1.1 Effects of Seawater Eddies on Charging Systems

Compared to traditional wireless charging technology in air medium, the key distinction in wirelessly charging AUVs underwater lies in the completely different medium between the transmitter and receiver sides of the magnetic coupler. Table 1 presents the relevant electromagnetic parameters in different mediums. Due to the significant differences in electromagnetic parameters between the marine environment and air medium, there exist substantial distinctions in the energy transfer models and their transmission characteristics under these two operational conditions.

Table 1. Electromagnetic Parameters in Different Media

Medium	Relative Permittivity	Electrical Conductivity	Relative Magnetic Permeability
Air	1.006	0	1.000004

Water	81	0.01	0.999991
Seawater	81	4	0.999991

Underwater wireless charging systems operate based on the fundamental principle of electromagnetic coupling. Alternating current in the coil generates an alternating magnetic field in space. Due to the significantly higher relative permittivity and electrical conductivity of seawater compared to air, vortex currents are induced in the water, creating an eddy current electric field. The presence of this electric field induces electromotive forces in the original circuit, thereby affecting the circuit parameters and causing a decline in energy transfer efficiency. To more effectively analyze the impact of eddy currents on wireless charging systems, an illustrative diagram of the electric field eddy current, as shown in Figure 1, is established.

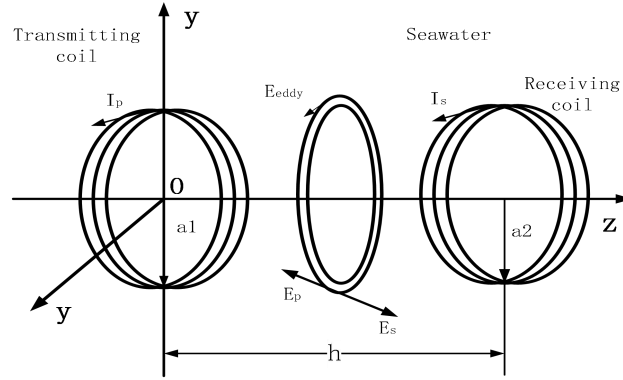


Fig.1 Electric Field and Eddy Currents Formed by Wireless Charging in Seawater

Assuming the radius of the magnetic coupler coil is 'a' and the current flowing through it is $i(t) = \sqrt{2}I \cos(\omega t + \theta_1)$. To simplify the model, let's assume that seawater is isotropic. We use ϵ to represent the permittivity of seawater, μ to represent the relative magnetic permeability, and σ to represent the electrical conductivity of seawater. The electric field strength at any point in seawater is given by [13]:

$$E(\rho, \varphi, z) = -\frac{j\omega\mu a I}{2} \int_0^\infty \frac{\lambda}{u} J_1(\lambda a) J_1(\lambda \rho) e^{-u|z|} d\lambda e_\varphi \quad (1)$$

Here, $E(\rho, \varphi, z)$ is the complex vector representation of the electric field strength at point Q, $u = \sqrt{\lambda^2 - \omega\mu(\epsilon - j\sigma)}$, ω is the current frequency, λ is the integration variable, I is the current in the coil, $J_1(x)$ is the first-order Bessel function, e_φ is the unit directional vector of the electric field strength, and its direction is tangential to the loop of the induced electric field.

If we denote the distance between the transmitting and receiving sides as 'h', then the composite magnetic field at point Q can be expressed as:

$$E_{\text{eddy}}(\rho, \varphi, z) = E_p(\rho, \varphi, z) + E_s(\rho, \varphi, z) \quad (2)$$

Here, E_p and E_s represent the electric fields generated by the currents in the transmitting and receiving sides, respectively, at point $Q(\rho, \varphi, z)$.

The power loss due to eddy current in the wireless charging system in seawater can be calculated as:

$$P_{\text{eddy}} = \iiint_V \sigma E_{\text{eddy}}^2 dV \quad (3)$$

It can be expressed when the currents in the transmitting and receiving coils differ by 90 degrees:

$$E_{\text{eddy}}^2 \approx E_p^2 + E_s^2 \quad (4)$$

Further derivation yields:

$$P_{\text{eddy}} = \iiint_V \sigma (E_p^2 + E_s^2) dV \quad (5)$$

It can be observed that a portion of the eddy current loss in seawater is generated by the electric field E_P formed by the current in the transmitting coil, and another portion is generated by the electric field E_S formed by the induced current in the receiving coil. Since these two parts do not affect each other and are only related to the currents on their respective sides, the eddy current losses on the transmitting and receiving sides can be equivalently represented as energy dissipation on series resistances on both sides. The series resistances on the transmitting and receiving sides are respectively:

$$R_{\text{eddy1}} = \frac{\iiint_V \sigma E_P^2 dV}{I_P^2} \quad (6)$$

$$R_{\text{eddy2}} = \frac{\iiint_V \sigma E_S^2 dV}{I_S^2} \quad (7)$$

2.1.2 Equivalent Model of Wireless Charging System

Typically, a wireless charging system consists of an inverter, transmitting side compensation network, magnetic coupler, receiving side compensation network, rectifier bridge, and voltage reduction module.

When the magnetic coupler structure is transferring energy, induced currents will be generated in the transmitting coil on the transmitting side, impacting the system. Additionally, due to the inherent inductance of the coil, if compensation components are not introduced into the circuit, the circuit exhibits inductive impedance, causing the current in the circuit to lag behind the voltage phase. This results in lower active power and a smaller power factor. Therefore, series or parallel capacitor-inductor components need to be introduced to form a compensation topology.

Traditional WPT systems have four basic compensation structures: S-S type, S-P type, P-S type, and P-P type. Due to its simple network structure and the characteristic that the resonant frequency does not change with variations in load and mutual inductance, the S-S type is often chosen. Moreover, the improved LCC-S type compensation network based on the S-S type can quantitatively express the magnitude of eddy current losses in seawater and correct system detuning. Therefore, this paper adopts the LCC-S compensation network structure as the compensation network for the wireless charging system. Figure 2 shows the corresponding equivalent model of the system.

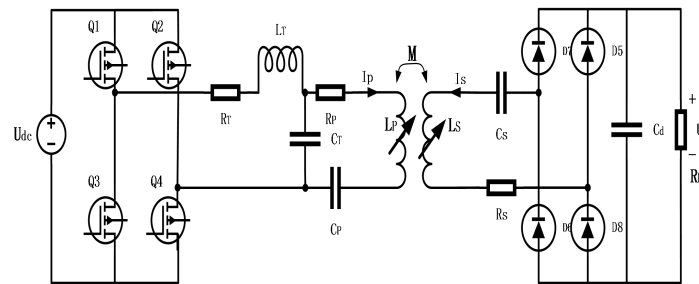


Fig. 2 Equivalent Model of Wireless Charging System

Where L_P and L_S are the self-inductances of the transmitting and receiving coils, respectively; M is the mutual inductance between the two coils; C_P , C_T , and C_S are compensation capacitors, connected in series with the transmitting coil, in parallel with the receiving coil, and in series with the receiving coil, respectively; R_T is the impedance matching resistor; R_P is the equivalent series resistance of the transmitting coil, and R_S is the equivalent series resistance of the receiving coil; R_L is the load resistor; I_P and I_S are the effective values of the currents in the transmitting and receiving coils, respectively. According to the equivalent model, the loop impedances on the transmitting (Z_P) and receiving (Z_S) sides can be calculated as:

$$Z_s = R_s + R_L + \frac{1}{j\omega C_s} + j\omega L_s \quad (8)$$

$$Z_p = R_p + R_T + \frac{1}{j\omega C_p + \frac{1}{j\omega L_p + 1/j\omega C_r + Z_{sp}}} \quad (9)$$

Where $Z_{sp} = \frac{\omega M}{Z_s}$ is the reflected impedance on the receiving side seen from the transmitting side.

Transmission power and actual power transmission efficiency can be derived as:

$$P_L = \text{Re}\{V_L \cdot I_p^*\} = \frac{\omega^2 \cdot M^2 \cdot R_L \cdot I_p \cdot I_s^*}{Z_p \cdot Z_s^*} \quad (10)$$

$$\eta = \frac{\text{Re}\{V_L \cdot I_p^*\}}{\text{Re}\{V_s \cdot I_s^*\}} = \frac{\omega^2 M^2 \cdot R_L}{\text{Re}\{Z_s \cdot Z_p \cdot Z_p^* + \omega^2 M^2 \cdot Z_p^*\}} \quad (11)$$

It can be observed that to improve the charging efficiency, it is necessary to increase the mutual inductance M between the two coils. The relationship between mutual inductance and coupling coefficient k is as follows:

$$k = \frac{|M|}{\sqrt{L_p L_s}} \quad (12)$$

When the coils are determined, L_p and L_s are fixed constants. As indicated in equation (12), the coil's mutual inductance can be enhanced by increasing the coupling coefficient between the coils on both sides of the magnetic coupler, thereby improving the system's charging efficiency. Therefore, this paper considers enhancing the coupling coefficient as the primary goal in the design of the magnetic coupler.

2.2 Magnetic Coupler Structural Design

Considering the advantages of radial misalignment compensation in the magnetic coupling loop with DD coils, this paper adopts DD coils as the coil type for the coupler. The magnetic field zoning calculation formula, which guides the design of the coupler by assessing the impact on the coupling coefficient, is employed. Figure 3 illustrates the magnetic field zoning of the DD-type magnetic coupler.

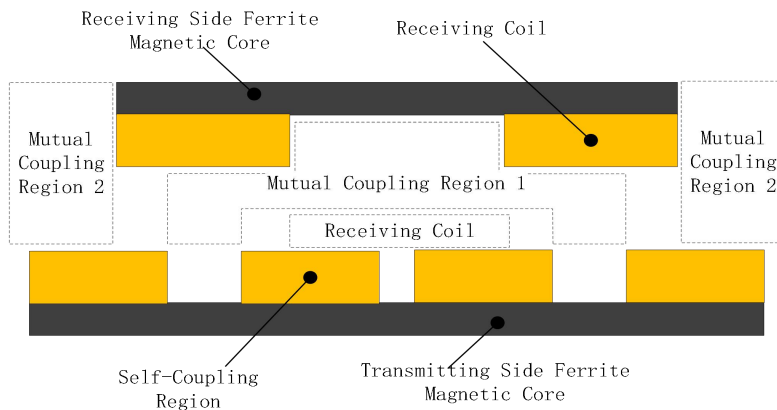


Fig. 3 Based on DD-Type Coil Coupling Magnetic Field Zoning Diagram

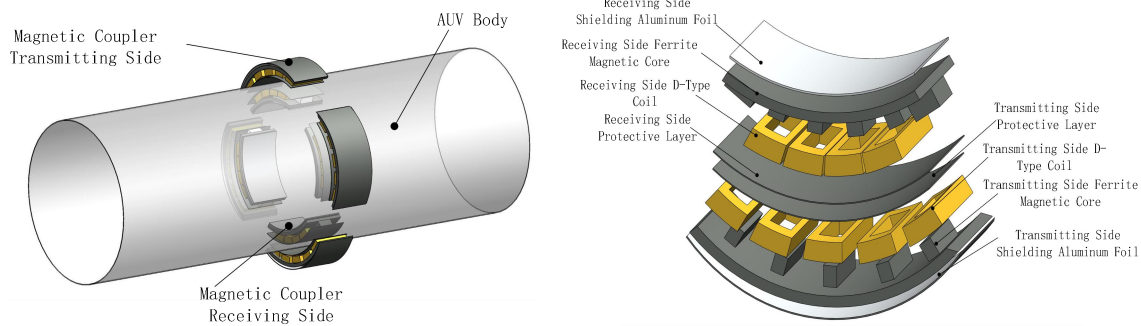
In the magnetic coupling loop, let R_s be the self-coupling reluctance, R_{m1} and R_{m2} be the reluctances of mutual coupling regions 1 and 2, Φ_s be the magnetic flux in the self-coupling region, and Φ_m be the magnetic flux in the mutual coupling region. Therefore, based on the expression for magnetic flux with respect to the coupling coefficient, the design formula for the coupling coefficient of the DD coil's magnetic flux can be derived as [14]:

$$k = \frac{\Phi_m}{\Phi_s + \Phi_m} = \frac{R_s / (R_{m1} + R_{m2})}{R_{m1} + R_{m2}} = \frac{1}{1 + \frac{R_{m1} + R_{m2}}{R_s}} \quad (13)$$

It can be seen that increasing R_s or decreasing R_{m1} and R_{m2} can both enhance the coil's coupling coefficient. Due to the high magnetic permeability of the magnetic core, combining the magnetic field zoning shown in Figure 3, adding a ferrite magnetic core in the mutual coupling region of the magnetic coupler can reduce the magnetic reluctance in the mutual coupling region, ultimately increasing the coil's coupling coefficient.

Considering the cylindrical structure characteristics of the AUV hull, and from the perspective of the compatibility between the magnetic field distribution on the transmitting and receiving sides of the magnetic coupler and the mechanical structure, this paper designs a magnetic coupler with arc characteristics, composed of multiple D-type coils, as shown in Figure 4. Figure 4(a) is a schematic diagram of four sets of magnetic couplers uniformly distributed at 90 degrees on the AUV shell, and Figure 4(b) is an internal expanded view of a single set of magnetic couplers.

The transmitting part includes a protective layer on the transmitting side, D-type coils on the transmitting side, a ferrite magnetic core on the transmitting side, and shielding aluminum foil on the transmitting side, with cylindrical ferromagnetic blocks located on the side near the center. The receiving part includes a protective layer on the receiving side, D-type coils on the receiving side, a ferrite magnetic core on the receiving side, and shielding aluminum foil on the receiving side, with cylindrical ferromagnetic blocks located on the side away from the center. Each pair of adjacent coils on the transmitting side forms a DD coil pair, and each coil pair on the transmitting side is always coupled with one D-type coil on the receiving side. The ferromagnetic core enhances the energy transfer capability of the magnetic flux circuit in the mutual coupling region, contributing to an increase in the coupling coefficient and providing certain offset tolerance capabilities [15]. Additionally, the magnetic coupler designed in this paper uses conventional aluminum foil as the leakage magnetic shielding layer to improve the anti-leakage magnetic performance of the magnetic coupler [16-17].



(a) External Structure of the Magnetic Coupler (b) Exploded View of a Single Set of Couplers
Fig.4 Magnetic Coupler Structure

3. Determination of Structural Parameters for the Magnetic Coupler

The determination of structural parameters for the magnetic coupler is crucial for enhancing the coupling coefficient. As the design of magnetic coupler parameters is a multi-dimensional function problem, neural network algorithms are widely used in the multi-objective parameter design field. Neural network algorithms have the advantages of non-linear mapping capability and strong fault tolerance. However, a standalone neural network model usually requires setting multiple hyperparameters, such as the number of hidden layer nodes, activation functions, and learning rates. These hyperparameters directly affect the experimental performance of the model, and adjusting hyperparameters typically involves manual and automatic methods. Manual adjustment of

hyperparameters is susceptible to subjective biases and faces issues of local optima and overfitting. Therefore, an efficient automatic hyperparameter tuning method is crucial for improving the performance and training efficiency of neural network models. Genetic algorithms have good robustness and powerful parallelization capabilities. Combining the advantages of genetic algorithms in optimizing the weights and biases of BP neural networks for parameter prediction, this paper integrates and applies both algorithms in the determination of magnetic coupler structural parameters.

The BP neural network used in this paper has the following input layer parameters: initial coil inner diameter, coil turns, width of the ferrite, arc length of the ferrite, and height of the cylindrical ferromagnetic block. The hidden layer contains five neurons, the output layer represents the coupling coefficient value, and the genetic algorithm is iteratively applied to adjust the weights and thresholds of the BP neural network based on the comparison error between the current coupling coefficient value and the target coupling coefficient value. The convergence of the genetic algorithm is used to determine the final weights and thresholds. The corresponding objective function includes the product of the original parameters and biases. The algorithm flowchart is shown in Figure 5.

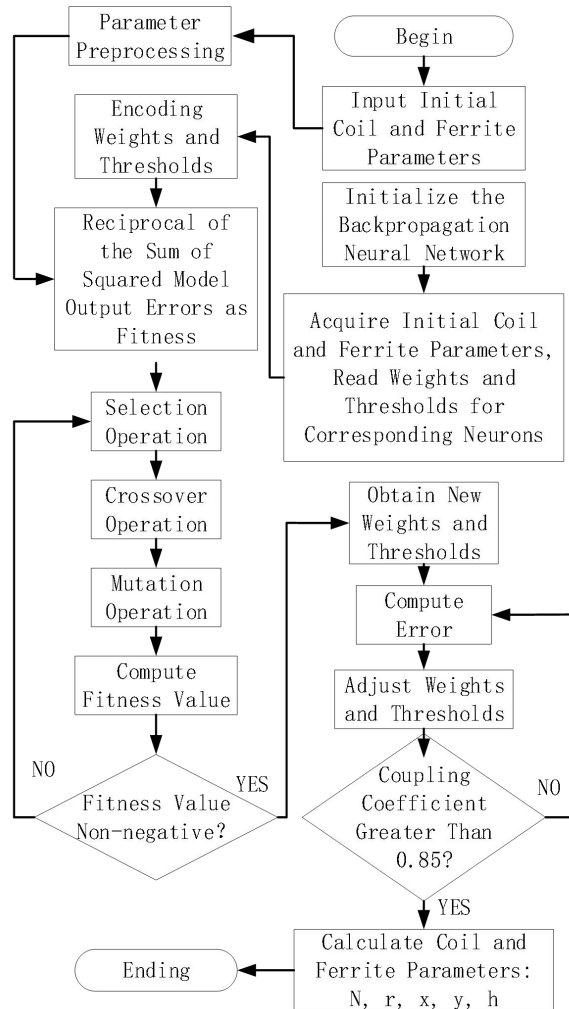


Fig. 5 Genetic-BP Neural Network Algorithm Flowchart

In this paper, the geometric parameters of the magnetic coupler are determined based on the outer diameter parameters of the PX-324 series medium-sized AUV. The inner diameter of the transmitting side is 350mm, and the outer diameter is 450mm, while the inner diameter of the receiving side is 230mm, and the outer diameter is 300mm. The power of the designed wireless charging system is 250W, and the parameters of the Liz wire are shown in Table 2, wound in a cylindrical spiral coil. The magnetic core material used is ferrite, and the shielding layer is made of

aluminum foil. Genetic algorithms are employed to optimize the parameters of biases and weights in the BP neural network. The optimized BP neural network is then used to determine the parameters of the magnetic coupler coils, such as inner and outer diameters, turns, and the thickness and width of the ferrite.

Table 2. Liz wire parameters

Parameters	Single-strand wire diameter/mm	Strand count	Outer diameter /mm	Cross-sectional area /mm ²	Ampacity /A
value	0.1	130	1.6	1.02	5.1

In order to achieve the required power for the designed wireless charging system and effectively improve wireless charging efficiency, it is necessary to set the coupling coefficient of the magnetic coupler to the target value while minimizing the mass of the magnetic coupler. In this paper, with the primary goal of achieving a coupling coefficient of 0.85, and the coil and ferrite mass as secondary objectives, the parameters of the coil winding and the geometric parameters of the ferrite are optimized. The objective function designed is:

$$F = \alpha f_1(r_{coil}, N, x, y, h_{Fe}) + \beta f_2(r_{coil}, N, x, y, h_{Fe})$$

Where f_1 is the objective function for the coupling coefficient value of the magnetic coupler, f_2 is the objective function for the mass of the magnetic coupler, α and β are the weight coefficients of the two objective functions, r_{coil} is the inner diameter of the coil, N is the number of turns of the coil, x and y are the width and arc length of the ferrite section, and $x=y$, indicating a square section. h is the height of the ferrite block. In this paper, since the coil is directly wound around the ferrite block with a square section, the ferrite can be considered as the inscribed square when the coil is wound in a circular manner. Thus, the side length of the block-shaped ferrite is taken as $\frac{r_{coil}}{\sqrt{2}}$.

In addition, to avoid interference at the end near the center caused by the height of the ferrite being too high during circular distribution, the height of the ferrite and the outer diameter of the coil should satisfy the following conditions:

$$h \leq \frac{r^*}{4}, \quad r_{coil} \leq \frac{\pi \cdot r^*}{10} \quad (14)$$

Where r^* is the inner radius of the coupler, taking 400mm for the transmitter side and 265mm for the receiver side.

In this algorithm, the selected fitness function is the reciprocal of the sum of squared errors, i.e.:

$$E = \sum_{j=1}^n (P_j^{k-1}(w, x) - y_j)^2 \quad (15)$$

$$F(j) = \frac{1}{E(j)} \quad (16)$$

Where E is the error function, P is the overall output, w is the weight vector, x is the input vector, y is the output vector, F is the fitness, and j is the iteration number. Figure 6 depicts the iterative process of the genetic optimization BP neural network. It can be seen that after 447 rounds of iteration, the algorithm eventually tends to converge. At this point, the corresponding coil inner diameter parameters are 84.28mm, the coil turns are 35.7 turns, the width of the ferrite is 81.36mm, and the height of the ferrite is 71.40mm.

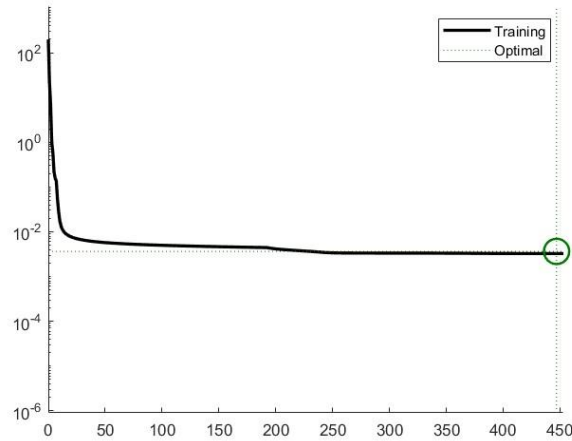


Figure 6 Algorithm Iterative Convergence Process

4. Electromagnetic Field Simulation Analysis

In order to validate the rationality of the parameters of the magnetic coupler and investigate the potential adverse effects of misalignment during AUV charging on the coupling coefficient, this section conducts electromagnetic field simulation analysis on the magnetic coupler using ANSYS MAXWELL. Specifically, two scenarios are considered: one with a radial offset of 10mm and the other with a circumferential rotation offset of 5° on the transmission side relative to the receiving side. Each scenario is simulated 20 times, and the magnetic coupling coefficient is recorded for each experiment.

In the electromagnetic field simulation, a solving domain surrounding the model is set up with an expansion factor of 100% for the solution model. The simulation type is set to static magnetic field simulation, and the boundary conditions are set to two-dimensional Vector Potential. The mesh is refined based on length, and the core material is set to ferrite, while the coil material is set to copper. The simulation input voltage on the transmission side is 72V with a frequency of 40kHz, and the shielding layer material is Al₂O₃.

The simulation results are depicted in the contour plots in Figure 7. When excitation is applied to the transmission side of a single magnetic coupler, the magnetic field is evenly distributed on the side near the center of the magnetic coupler and around each coil group. The simulation vector plots in Figure 8 show that, when the transmission side and receiving side are coordinated, coherent magnetic coupling vectors are formed that penetrate both the transmission and receiving sides of the magnetic coupler.

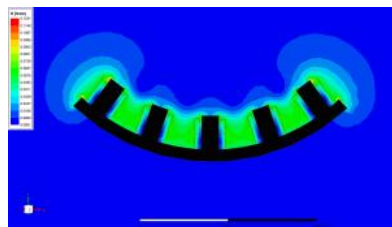


Fig. 7 Simulation Cloud Map of the Magnetic Field on the Emission Side

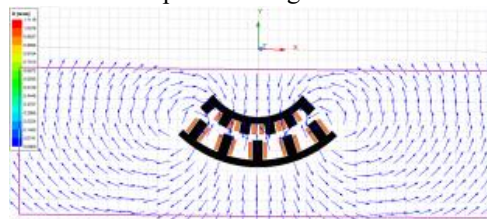


Fig. 8 Magnetic Coupler Magnetic Field Simulation Vector Map

In order to study the variation of the coupling coefficient in the offset experiment of the designed magnetic coupler in this paper, a group of simulation control experiments of magnetic coupling at the central symmetrical position need to be conducted in advance. The magnetic field distribution cloud map at this time is shown in Figure 9, where the receiving side and the emission side of the magnetic coupler are in the centrally symmetrical ideal coupling position. It can be seen that the positions with higher concentration of magnetic flux distribution are the coil coupling positions, and the overall external and internal distribution of magnetic flux in the coupler is relatively low. This can minimize the interference of the magnetic field of the coupler with the internal electronic components of the AUV. The coupling coefficient at the ideal position is 0.87.

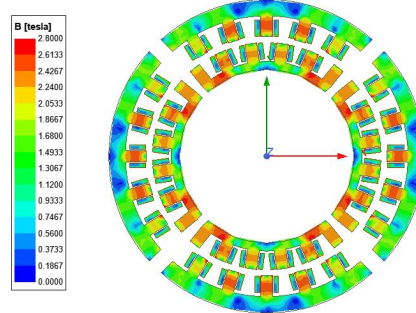


Fig.9 Central Symmetric Coupling Magnetic Field Distribution Cloud Map

Firstly, the first set of experiments with a 10mm offset in the radial direction between the receiving and transmitting sides of the magnetic coupler were conducted. The magnetic field distribution cloud map after the offset is shown in Figure 10.

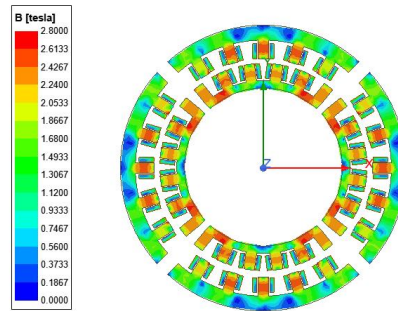


Fig.10 Magnetic Field Cloud Map with 10mm Radial Offset

During the offset process, 20 sets of coupling coefficient data about the offset distance were recorded with a step size of 0.5mm. The overall coupling coefficient decreased from the original 0.87 to 0.74, and the variation curve is shown in Figure 11. It can be observed that the coupling coefficient decreases gradually when the offset is less than 4.5mm, and the decrease becomes more rapid when the offset exceeds 4.5mm. This indicates that the magnetic coupler has a certain fault-tolerant capability for radial offset within 4.5mm.

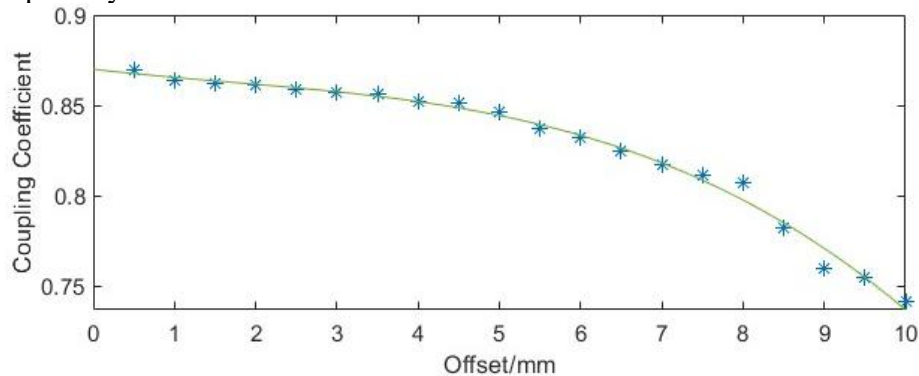


Fig.11 Variation of Coupling Coefficient with Radial Offset

Next, the second set of simulations was conducted with a 5° offset in the circumferential direction between the receiving and transmitting sides of the magnetic coupler. The magnetic field distribution cloud map after the offset is shown in Figure 12.

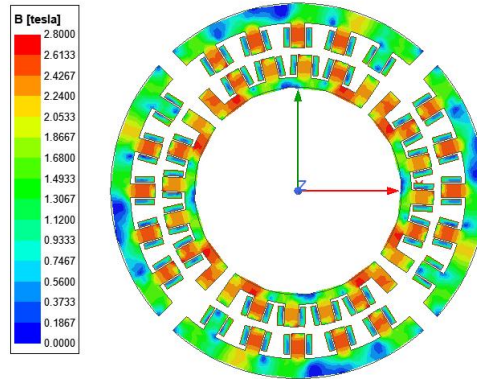


Fig.12 Magnetic Field Cloud Map with 5° Circumferential Offset

During the offset process, 20 sets of coupling coefficient data about the offset angle were recorded with a step size of 0.25° . The overall coupling coefficient decreased from the original 0.87 to 0.78, and the variation curve is shown in Figure 13. It can be observed that the coupling coefficient remains above 0.8 during the offset of 0° to 4° . However, after the offset exceeds 4° , the coupling coefficient shows an accelerated decline. This indicates that the magnetic coupler has a certain fault-tolerant capability for circumferential offset within 0° to 4° .

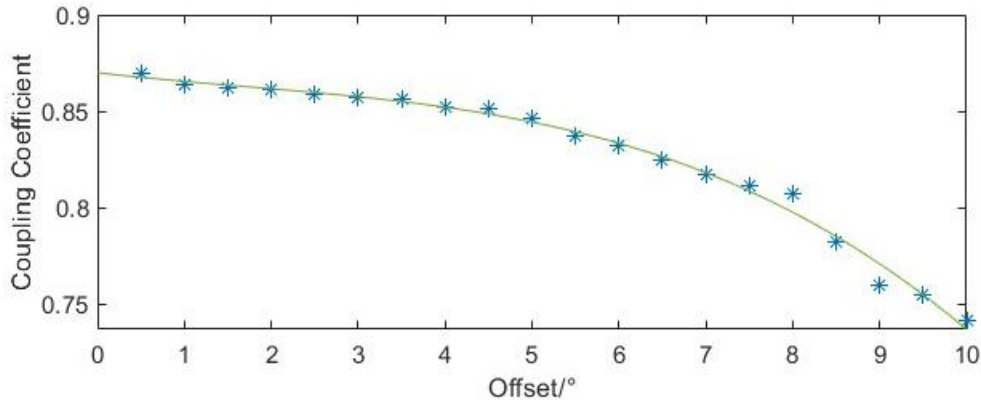


Fig.13 Variation of Coupling Coefficient with Circumferential Offset

5. Summary

This paper focuses on the research of the AUV wireless charging system and designs a magnetic coupler consisting of multiple D-shaped coils with radial and circumferential offset simulations conducted in the ANSYS MAXWELL environment.

1. Analyzing the impact of eddy current phenomena in seawater conditions on the wireless charging system, the efficiency of the wireless charging system is related to the coupling coefficient of the magnetic coupler. Improving the coupling coefficient can enhance the charging efficiency.

2. Using DD-type coils as the winding type for the magnetic coupler, the coupling coefficient formula derived from the magnetic resistance of the coupler indicates that designing a coupler with a high coupling coefficient can be achieved by adjusting the position of the magnetic core to increase permeability and reduce magnetic resistance.

3. Employing a genetic algorithm combined with a backpropagation neural network (BPNN) algorithm to optimize the structural parameters of coils and ferrites, with coupling coefficient value and coupler mass as objective functions. Radial and circumferential offset simulations conducted in

the ANSYS MAXWELL environment demonstrated good fault tolerance in the 0~4.5mm radial offset range and a certain degree of fault tolerance in the $0^{\circ} \sim 4^{\circ}$ circumferential offset range.

References

- [1] Abou Houran M, Yang X, Chen W. Magnetically coupled resonance WPT: Review of compensation topologies, resonator structures with misalignment, and EMI diagnostics[J]. *Electronics*, 2018, 7(11): 296.
- [2] Zhang B, Chen J, Wang X, et al. High-Power-Density Wireless Power Transfer System for Autonomous Underwater Vehicle Based on a Variable Ring-Shaped Magnetic Coupler[J]. *IEEE Transactions on Transportation Electrification*, 2023.
- [3] Lyu F, Cai T, Huang F. A universal wireless charging platform with novel bulged-structure transmitter design for multiple heterogeneous autonomous underwater vehicles (AUVs)[J]. *IET Power Electronics*, 2023.
- [4] Lin M, Lin R, Li D, et al. Development of a Radially Coupled Wireless Charging System for Torpedo-Shaped Autonomous Underwater Vehicles[J]. *Journal of Marine Science and Engineering*, 2023, 11(6): 1180.
- [5] Zhang B, Wang X, Lu C, et al. A wireless power transfer system for an autonomous underwater vehicle based on lightweight universal variable ring-shaped magnetic coupling[J]. *International Journal of Circuit Theory and Applications*, 2023.
- [6] Xia T, Li H, Yu H, et al. A Circular-Arc-Type Magnetic Coupler with Strong Misalignment Tolerance for AUV Wireless Charging System[J]. *Journal of Marine Science and Engineering*, 2023, 11(1): 162.
- [7] Kan T, Mai R, Mercier P P, et al. Design and analysis of a three-phase wireless charging system for lightweight autonomous underwater vehicles[J]. *IEEE Transactions on power electronics*, 2017, 33(8): 6622-6632.
- [8] Teeneti C R, Truscott T T, Beal D N, et al. Review of wireless charging systems for autonomous underwater vehicles[J]. *IEEE Journal of Oceanic Engineering*, 2019, 46(1): 68-87.
- [9] Agostinho L R, Ricardo N C, Silva R J, et al. A Modular Inductive Wireless Charging Solution for Autonomous Underwater Vehicles[C]//2021 IEEE International Conference on Autonomous Robot Systems and Competitions (ICARSC). IEEE, 2021: 68-73.
- [10] Wang Zhongda. Design of Magnetic Coupling Wireless Charging System for Autonomous Underwater Vehicles [D]. Dalian: Dalian University of Technology, 2022.
- [11] Qin Mu. Research on Magnetic Induction Coupling Wireless Charging Technology for Underwater Autonomous Vehicles [D]. Harbin: Harbin Institute of Technology, 2019.
- [12] Cai C, Zhang Y, Wu S, et al. A circumferential coupled dipole-coil magnetic coupler for autonomous underwater vehicles wireless charging applications[J]. *IEEE Access*, 2020, 8: 65432-65442.
- [13] Liu Yuxin, Gao Fei, Liu Xin, et al. Analysis of Eddy Current Loss and Efficiency Optimization in Deep-Sea Unmanned Underwater Vehicle Bidirectional Wireless Charging System [J/OL]. *Journal of Electrical Engineering*. <https://doi.org/10.19595/j.cnki.1000-6753.tces.231122>.
- [14] Liu Zhizhen, Zeng Hao, Chen Hongxing, et al. Design and Optimization of Core Structure for Wireless Charging System of Electric Vehicles [J]. *Journal of Electric Machines and Control*, 2018, 22(1): 8-15.
- [15] Budhia M, Covic G A, Boys J T. Design and optimization of circular magnetic structures for lumped inductive power transfer systems[J]. *IEEE Transactions on Power Electronics*, 2011, 26(11): 3096-3108.
- [16] Budhia M, Boys J T, Covic G A, et al. Development of a single-sided flux magnetic coupler for electric vehicle IPT charging systems[J]. *IEEE Transactions on Industrial Electronics*, 2011, 60(1): 318-328.
- [17] Lu Zhe, Wang Chunfang, Yang Lingyun, et al. Wireless Charging Coupler for Electric Vehicles with Composite Shielding Layer [J]. *Journal of Power Supply*, 2022, 20(6): 75-83.